Molecular Simulation of Sucrose Solutions near the Glass Transition Temperature

Nancy C. Ekdawi-Sever, Paul B. Conrad, and Juan J. de Pablo*

Department of Chemical Engineering, University of Wisconsin-Madison, 1415 Engineering Drive, Madison, Wisconsin 53706

Received: July 31, 2000; In Final Form: November 9, 2000

The physical properties of aqueous sucrose near the glass transition temperature have been studied using Monte Carlo and molecular dynamics simulations. The sucrose solutions ranged in concentration from 6 to 100 wt% and in temperature from 300 to 600 K. For concentrated solutions (≥ 80 wt%), a parallel tempering Monte Carlo algorithm was implemented to circumvent the slow system dynamics and improve sampling of configuration space. Parallel-tempered density calculations agree more closely with experimental data than conventional NPT results. Our simulations indicate that aqueous sucrose retains two intramolecular hydrogen bonds even in dilute solutions. The two hydrogen bonds detected in crystalline sucrose were also observed in the sucrose solutions of 50 wt% sucrose and greater. The hydration number was calculated for sucrose and compared with that for trehalose. Sucrose is less hydrated than trehalose for all concentrations studied. Using parallel-tempered NPT density results, molecular dynamics simulations were utilized to estimate the diffusion of water near the glass transition for concentrated sugar solutions. Diffusion coefficients in aqueous sucrose appear to be a factor of 2 greater than those in trehalose solutions.

1. Introduction

Disaccharides have been shown to be effective cryoprotectants for biological systems. Sugars added to aqueous biological samples (i.e., cells, lipid membranes, or proteins) prior to freeze-drying or dehydration can improve the activity of biomaterial upon thawing or rehydration.[1−3] The primary drying phase of lyophilization (freeze-drying) is a two-step process in which the aqueous biological sample is frozen and, subsequently, ice crystals are sublimed. Because pure ice crystals form during the freezing step, the amount of water that remains in the solution near the biomaterial decreases significantly. As water is removed from the vicinity of the biological material, the concentration of ions and sugars increases. The water replacement hypothesis[4] contends that the observed carbohydrate-induced stability of dehydrated biologicals is partially due to specific favorable interactions (i.e., hydrogen bonding) between the sugar and the biological material.

Furthermore, concentrated sugar solutions can form glasses at room temperature. Sugar glasses can be prepared by freeze-drying and dehydration processes. Glasses are often defined as metastable states in which large-scale molecular motion is almost negligible, and where the longest relaxation times exceed laboratory time scales.[5] The presence of a glassy matrix, therefore, hinders the motion of the biomaterial and its environment. This type of kinetic arrest reduces the rate of small-molecule diffusion to and from the cells and of biomolecular conformational changes. It is believed that osmotic stresses and physical damage through crystallization are some of the more important reasons for cell death during freezing and drying.[6] These processes can be partially alleviated by quenching highly viscous sugar solutions. Consequently, storage in a glassy matrix could reduce the loss of biological activity over time.

The disaccharides sucrose and α,α-trehalose (referred to as trehalose), among others, have been identified as effective stabilizers of biologicals in the freeze-dried and dehydrated state.[7−9] The structures of these two sugars are shown in Figures 1 and 2. While sucrose has been used extensively by the pharmaceutical industry for lyophilization, an increasing body of literature suggest that trehalose might have some advantages over sucrose.[1−3]

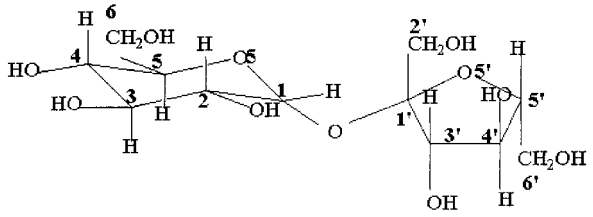

Figure 1. Sucrose − α-D-*Glucopyranosyl*, *β*-D-*fructofuranoside*.

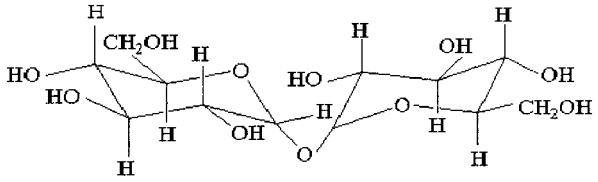

Figure 2. α,α-Trehalose − α-D-*Glucopyranosyl*, α-D-*glucopyranoside*

Sucrose and trehalose are nonreducing disaccharides with the same chemical formula ($C_{12}O_{11}H_{22}$) but slightly different structures. The sucrose molecule is composed of one fructose (5 carbons) and one glucose (6 carbons) ring, while trehalose is composed of two glucose rings. Both pure sugars form glasses at temperatures above ambient temperature, but the glass transition temperature for sucrose is significantly lower than that of trehalose (77 °C as opposed to 115 °C for trehalose).[10,11] Both disaccharides have been studied extensively; and their effects on biomaterials have been analyzed by numerous researchers. Several studies looked at the effect of sucrose on lipoproteins and enzymes. Work by Rumsey et al.[7] showed that sucrose prevented structural and functional changes during

* depablo@engr.wisc.edu

10.1021/jp002722i CCC: $20.00 © 2001 American Chemical Society
Published on Web 01/04/2001

freezing of low-density lipoproteins. Lee and Timasheff[9] studied the thermal transition of α-chymotrypsin, chymotrypsinogen, and ribonuclease in the presence and absence of sucrose. They found an increase in the denaturation temperature of these proteins which they attributed to an increase in the activation energy of denaturation. They argued that the presence of sucrose stabilizes proteins against thermal damage. Moreira et al.[8] studied the effect of sucrose and raffinose on lactate dehydrogenase and found that 100% of LDH was recovered after freeze-drying and storage for 8 h regardless of which sugar or which combination was used. However, as the storage time was increased, raffinose samples had higher activities. Several, studies comparing sucrose and trehalose have found increased stability in the trehalose systems.[1,2,12] In a study by Leslie et al., for example, freeze-dried *E. coli* and *B. thuringiensis* survival was 10% higher in trehalose than sucrose. Rossi et al. found that the enzyme EcoRI's activity was 3-fold higher in trehalose than in sucrose after storing at 45 °C for 21 days. The question then arises as to whether the use of sucrose instead of trehalose is advantageous, and under what circumstances could the latter be a better protectant. It is the aim of this work to explore the structure and dynamics of aqueous sucrose in an effort to identify those characteristics, if any, that make trehalose and sucrose different.

Computer simulations can provide valuable information on the structure and configuration of sucrose. Previous simulations of sucrose have looked at hydration and structure of sucrose in water using molecular mechanics and molecular dynamics.[13−15] These studies have focused on intramolecular hydrogen boding in dilute sucrose−water systems. Only a few studies on concentrated mono-saccharides have been performed.[15,16] These studies were limited by the size and slow dynamics of the systems. Only one study on concentrated disaccharides (namely trehalose) has appeared in the literature.[17] To the best of our knowledge, highly concentrated, near-glassy sucrose systems have not been previously studied. We are interested in studying these systems as models of the glassy matrix surrounding stabilized (freeze-dried or dehydrated) biomaterials. To alleviate some of the equilibration problems due to long relaxation times, we have implemented a parallel tempering technique.[18] Applying this technique to our fully flexible model allows us to study near-glassy sugar solutions. In previous work,[17] the properties of concentrated trehalose solutions were thoroughly studied using molecular simulations. In this work, we have conducted a detailed study of the structure of sucrose in aqueous solutions and compared the results to those obtained for trehalose.

2. Methods and Calculations

Our simulation employs a fully flexible atomistic model. The water model used is the flexible SPC[19] potential developed by Toukan and Rahman[20] which has been shown to describe the behavior of water reasonably well.[21] The model for the disaccharides consisted of intramolecular, Lennard−Jones 6−12, and Coulombic interactions. The bonded interactions were calculated using the OPLS[22] flexible model potential. The OPLS model, which was developed and optimized for carbohydrates, accounts for stretching, bending, and torsional forces. The Lennard−Jones cutoff radius was set at 7 Å and a long-range correction was applied to account for truncation errors. Long-range Coulombic interactions were calculated using a particle mesh Ewald (PME) algorithm.[23]

Both Monte Carlo and molecular dynamics simulations were used to calculate the properties of aqueous sucrose solutions. Table 1 describes the systems of varying concentrations which were simulated.

TABLE 1: Various Aqueous Sucrose Systems

concentration (wt%)	water molecules	sucrose molecules
6	300	1
20	152	2
50	76	4
80	29	6
90	17	8
100	0	10

Isothermal isobaric hybrid Monte Carlo (NPTMC) was used[24] with a multiple time scales algorithm (r-RESPA, see below) to enhance the equilibration of dense systems. As described by Mehlig et al., hybrid algorithms use molecular dynamics (MD) to move all the molecules in the system for a given amount of time (instead of the usual individual random particle selection and move). The molecules were allowed to move for five MD steps. The size of the time step was periodically adjusted to ensure a 70% acceptance ratio. Because the MD steps are within an MC algorithm, the hybrid simulation is exact regardless of time step size. The reversible reference system propagator algorithm (r-RESPA)[27] separates the forces into long-range and short-range. The short-range forces are updated more frequently than the long-range forces. In our simulations, the long-range time step was set at 5 times the short-range time step. This reduces the frequency of long-range calculations while keeping the algorithm exact. All NPTMC simulations ran for at least 1 million steps.

Isothermal molecular dynamics (NVTMD) simulations were used to calculate dynamic properties at different temperatures. The length of the runs depended on the number of molecules and the temperature. More steps were required to reach the free diffusion regime in higher density systems. All simulations ran for at least 5 ns with a step size of 0.25 fs; the density and starting configurations were determined from the NPTMC runs. Five Nosé-Hoover thermostats[25,26] were included to control the simulation temperature and a double r-RESPA[27] algorithm was implemented to speed up calculations. The double r-RESPA is a modification of the r-RESPA described above in which the velocity verlet algorithm is factorized into intramolecular (i.e., bonds, bending, and torsion), short-range (i.e., nonbonded interactions within the Lennard−Jones cutoff radius), and long-range (i.e., Coulombic) interactions. The bonded interactions were evaluated most often; the nonbonded and long-range forces were calculated every 2 and 4 MD steps, respectively.

To improve the density calculations at or below the glass transition temperature, a parallel tempering[18] algorithm was implemented. This method employs a number (n) of NPTMC simulation replicas running in parallel at different temperatures and pressures but with equal number of molecules. The replicas are arranged from 1 to n in order of increasing temperature and assigned an index i ($1 \leq i \leq n$). Periodically, random consecutive pairs of replicas (i and $i + 1$) are chosen and a swap trial move is attempted. In a swap move, the volume (V) and atomic configuration in replica i (C_i) are exchanged with those in replica $i+1$ (C_{i+1}). In other words

$$C_i^{\text{new}} = C_{i+1}^{\text{old}} \tag{1}$$

$$C_{i+1}^{\text{new}} = C_i^{\text{old}} \tag{2}$$

and

$$V_i^{\text{new}} = V_{i+1}^{\text{old}} \tag{3}$$

$$V_{i+1}^{\text{new}} = V_i^{\text{old}} \tag{4}$$

The acceptance criterion for conventional NPTMC is

$$P_{\mathrm{NPT}}^{\mathrm{acc}} = \min(1, e^{-\beta\Delta H}) \tag{5}$$

where

$$-\beta\Delta H = -\beta(U^{\mathrm{new}} - U^{\mathrm{old}}) - \beta(P^{\mathrm{new}}V^{\mathrm{new}} - P^{\mathrm{old}}V^{\mathrm{old}}) + Nln(V^{\mathrm{new}}/V^{\mathrm{old}})$$

and where U is the potential energy, V is the volume of the system, β is the inverse temperature ($1/k_{\mathrm{B}}T$), P is the pressure, and N is the number of molecules. In parallel tempering, the "*old*" volume and energies refer to the status of replica i and $i+1$ before a swap is attempted, and the "*new*" values are those of replica i and $i+1$ after the swap. (Note that, in this case, N is the same for all replicas.)

$$-\beta U^{\mathrm{new}} = -\beta_i U(C_i^{\mathrm{new}}) - \beta_{i+1} U(C_{i+1}^{\mathrm{new}}) \tag{6}$$

$$-\beta U^{\mathrm{old}} = -\beta_i U(C_i^{\mathrm{old}}) - \beta_{i+1} U(C_{i+1}^{\mathrm{old}}) \tag{7}$$

$$-\beta P^{\mathrm{new}}V^{\mathrm{new}} = -\beta P_i^{\mathrm{new}} V_i^{\mathrm{new}} - \beta P_{i+1}^{\mathrm{new}} V_{i+1}^{\mathrm{new}} \tag{8}$$

$$-\beta P^{\mathrm{old}}V^{\mathrm{old}} = -\beta P_i^{\mathrm{old}} V_i^{\mathrm{old}} - \beta P_{i+1}^{\mathrm{old}} V_{i+1}^{\mathrm{old}} \tag{9}$$

$$Nln\left(\frac{V^{\mathrm{new}}}{V^{\mathrm{old}}}\right) = 0 \tag{10}$$

The definitions in equations 6 through 10 are used in eq 5 to calculate $\beta\Delta H$. After some manipulations, the following acceptance criterion is derived for a trial swap move:

$$P_{\mathrm{NPT}}^{\mathrm{acc}} = \min(1, \mathrm{e}^{\Delta(\beta P)\Delta V + \Delta\beta\Delta U}) \tag{11}$$

where

$$\Delta(\beta P) = \beta_{i+1}P_{i+1} - \beta_i P_i$$

$$\Delta V = V_{i+1}^{\mathrm{old}} - V_i^{\mathrm{old}}$$

$$\Delta U = U_{i+1}^{\mathrm{old}} - U_i^{\mathrm{old}}$$

If the swap trial move is accepted, the simulation replicas are resumed from the new configurations. This method allows the lower temperature simulations to benefit from the faster motion attained at higher temperatures, thereby leading to faster equilibration. In addition, the swapping of configurations reduces the time spent in a local minimum and allows the system to explore configuration space more efficiently (see Figure 10 in the density section below).

In our simulations, we chose the replicas such that the temperatures were different but the pressures were fixed at 1 Bar. The acceptance criteria for this method is as follows

$$P_{\mathrm{NPT}}^{\mathrm{acc}} = \min(1, \mathrm{e}^{\mathbf{P}\Delta\beta\Delta V + \Delta\beta\Delta U}) \tag{12}$$

To ensure swapping between consecutive replicas, approximate energy histograms were calculated for different temperatures. If there was sufficient (10−20%) overlap between histograms at consecutive temperatures, then the corresponding simulation replicas had the possibility of swapping. If the histograms of two consecutive replicas did not overlap, then an intermediate temperature was added into the parallel tempering algorithm.

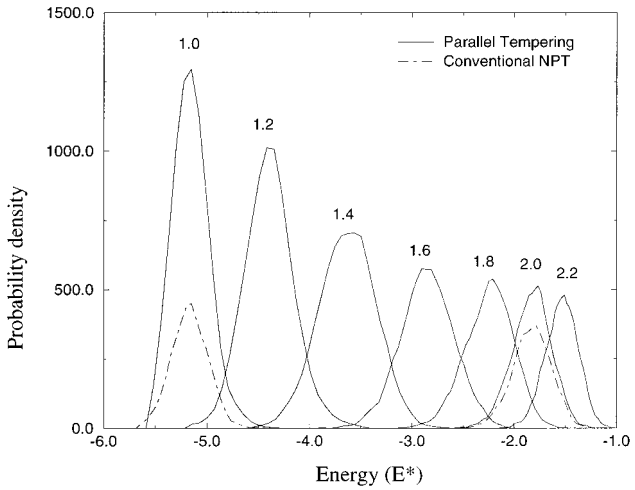

Figure 3. Energy histograms for Parallel NPTMC and conventional NPTMC for a Lennard−Jones fluid. The temperatures and energies are given in reduced units.

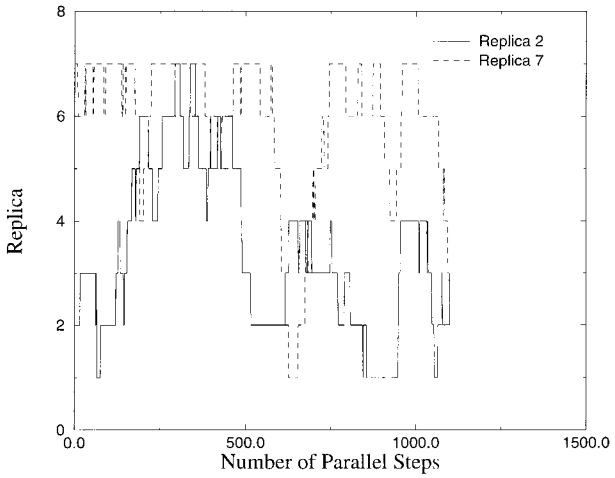

Figure 4. Paths of configurations as a function of time.

Parallel tempering was implemented first in an NPT ensemble of a Lennard−Jones (LJ) system of 108 particles. Figure 3 shows the energy histograms from a LJ parallel tempering simulation and those from conventional NPTMC data. The parallel tempering data correspond to a seven-replica parallel tempering run. The fact that the histograms of consecutive replicas overlap ensures that they can swap. Figure 3 compares the energy histograms at T^*=1.0 and $T^* = 2.0$ with and without tempering. Histograms corresponding to the same temperature are similar in that their maxima occur at the same value of energy (as they should), indicating that parallel tempering has not altered the system sampling. The heights of the distributions are different because the histograms were intentionally not normalized to enhance the comparison.

Figure 4 shows the trajectory of the initial configuration in two of the replicas as they swap from one replica to another. The unit of time here refers to a parallel step, which entails running all the simulation replicas for 100 MC hybrid steps and attempting a swap. The replicas are arranged in order of increasing temperature, with replica 1 having the lowest temperature. As can be seen in Figure 4, the configuration that began in replica 7 (the highest temperature) has swapped enough times to cover the entire range of temperatures. The configuration that began in replica 2 (second to lowest temperature) has also explored the entire range by swapping in and out of

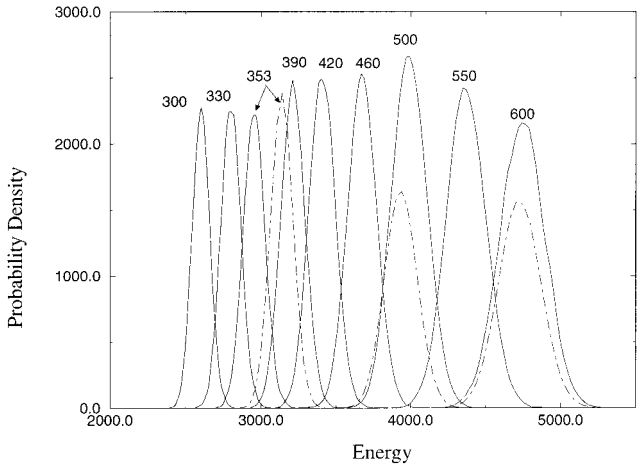

Figure 5. Energy histograms for Parallel NPTMC (solid line) and conventional NPTMC (dashed line) for a 100 wt% sucrose system.

all the replicas. From the point of view of a simulation replica at a given temperature, new configurations with different histories are constantly swapping in and out.

The sampling benefits of parallel tempering are particularly useful for systems with long relaxation times and high viscosities. Since we are simulating disaccharides near their glass transition temperature, these issues are particularly relevant. The paths of configurations for the sucrose system (data not shown) are similar to those shown in Figure 4. Figure 5 shows energy histograms for parallel tempering and conventional NPTMC sucrose simulations. At high temperatures, the histograms from the two methods are consistent. However, at lower temperatures (353 K), the histograms are significantly different. The energies and specific volume (see below) calculated using parallel tempering are lower than those obtained from conventional NPTMC simulations. This suggests that poor sampling using conventional NPTMC resulted in incorrect higher energies and lower densities at low temperatures. Parallel tempering yields better results by improving sampling of configurations that may not be accessible to conventional techniques.

3. Results and Discussion

3.1 Density. To verify the accuracy of our molecular simulations, the density of aqueous sucrose solutions was calculated as a function of composition and was compared to experimental data. Figure 6 shows both experimental[28] data and simulation results for the densities of sucrose solutions as a function of concentration. Low-density systems were simulated using conventional NPTMC, while high densities (80 wt% solutions and greater) used both parallel tempering and NPTMC. Note that conventional NPTMC becomes increasingly ineffective as the sucrose concentration increases; for pure sucrose, the difference in density for conventional and tempering simulations is as large as 4%, the latter value being much more reliable. To the best of our knowledge, no experimental data for pure amorphous sucrose at 353 K exists; Figure 6 shows the experimental density at ambient temperature.[29] It is expected that the density at 353 K would be slightly smaller than that at 298 K.

The improved simulation data attained at the higher density is an indication that parallel tempering is especially useful for dense and near-glassy systems. Figure 7 shows the density as a function of temperature for an 80 wt% sucrose system. The parallel tempering densities at the lower temperatures are in reasonable agreement with the experimental values, while the

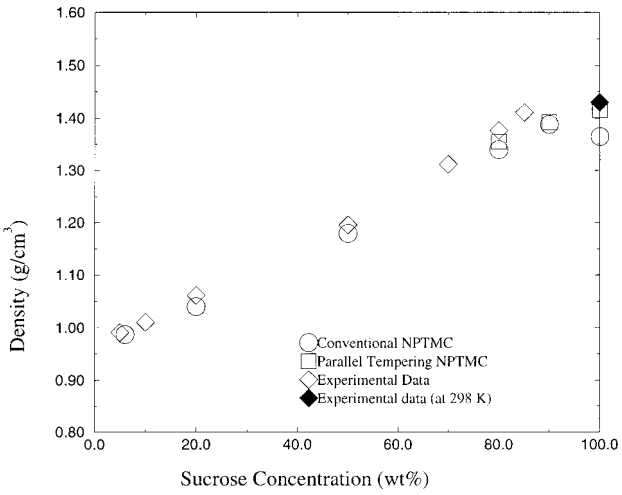

Figure 6. Density at 353 K of aqueous sucrose solutions as a function of concentration. Experimental data was taken from Mathlouthi et al.[28] Experimental data for amorphous sucrose at 298 K was obtained from Shamblin et al.[29]

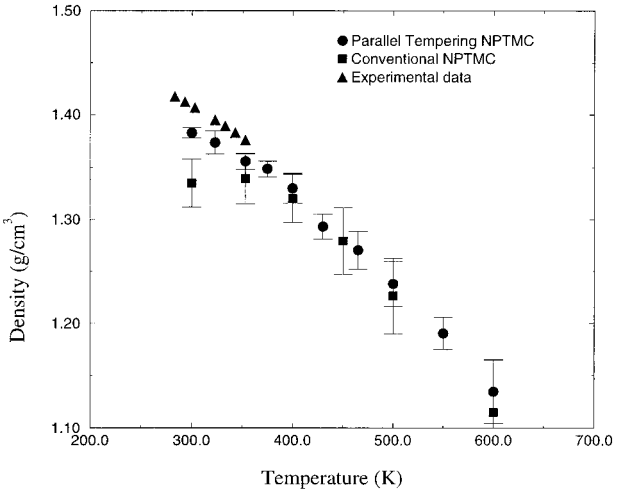

Figure 7. Comparison of calculated densities for an 80 wt% sucrose solution using parallel tempering and conventional NPTMC with experimental data.[28]

NPTMC densities are less accurate. For the 90 wt% and 100 wt% sucrose systems similar plots can be constructed; unfortunately, experimental data are not available. (Figures 8 and 9).

The glass transition temperature (T_g) has been determined experimentally for both trehalose and sucrose.[10] Using molecular simulations, it is difficult to calculate the transition because, at temperatures near and below T_g, the system dynamics are slow and equilibration times are inaccessible to conventional simulation methods. An apparent T_g can be estimated from the density curves by identifying the temperature at which there is an abrupt change in slope of the density curve. The three density curves shown in Figures 7, 8 and 9 do not show any definitive changes in the slope. We can speculate from this observation that the T_g occurs at a temperature below those simulated. This is consistent with experimental results which estimate T_g for 80 wt%, 90 wt% and pure sucrose at 233, 269, and 350 K, respectively.[30] It is important to note that using conventional NPTMC, T_g values of 425 and 500 K were estimated for the 80 wt% and pure sucrose systems, respectively.

The simulated densities for sucrose systems are consistently smaller than those calculated for trehalose.[17] For example, at 500 K, the densities for sucrose and trehalose are 1.366 g/cm^3,

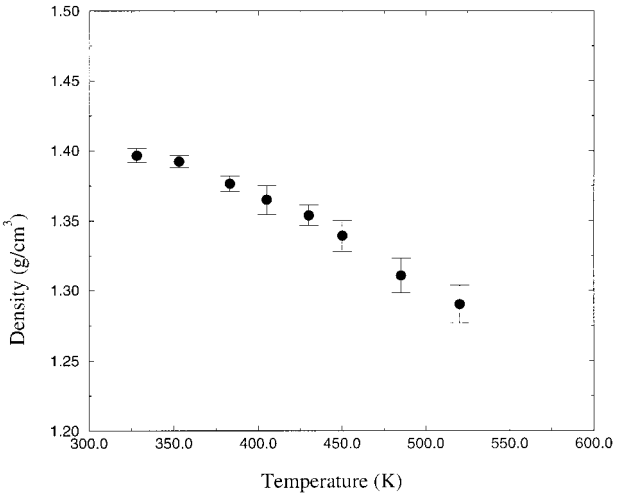

Figure 8. Predicted temperature dependence of density for a 90 wt% sucrose solution using parallel tempering.

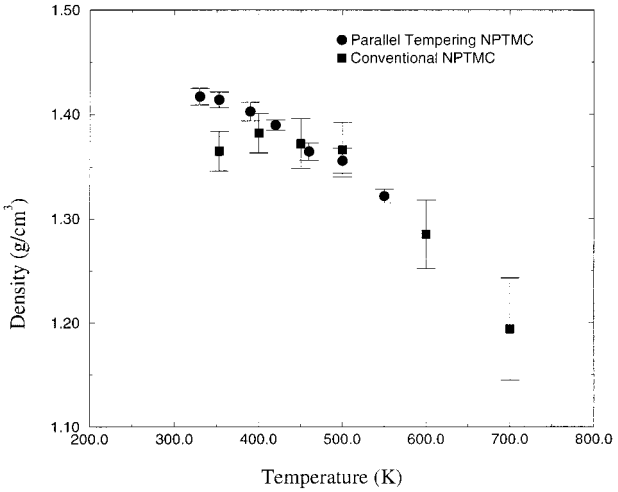

Figure 9. Comparison of the temperature dependence of density calculated using parallel tempering and conventional NPTMC for a pure sucrose system.

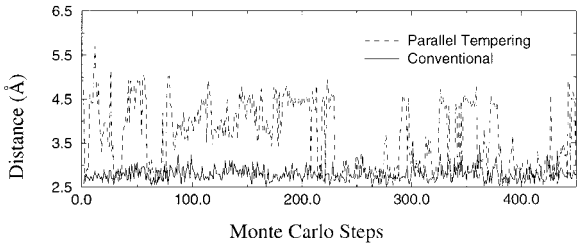

Figure 10. Distance between two oxygens (O6 and O5′) involved in hydrogen bonding using both parallel tempering and conventional NPTMC in an 80 wt% sucrose solution.

and 1.392 g/cm^3. The higher glass transition temperature observed in the trehalose systems can be attributed to the observed higher density.

3.2 Structure. *3.2.1 Intramolecular Structure.* Parallel tempering also improves calculations of structural properties because it increases the molecular motion of the disaccharides during a simulation. Figure 10 shows the distance between the two oxygens O6 and O5′ (see Figure 1) within a sucrose molecule in an 80 wt% solution; these two oxygens are involved in hydrogen bonding (see below), and their separation should oscillate between a value smaller than 3.4 Å and a value of 4.5 Å as the hydrogen bond forms and breaks. The figure depicts the separation over time for conventional NPTMC and parallel

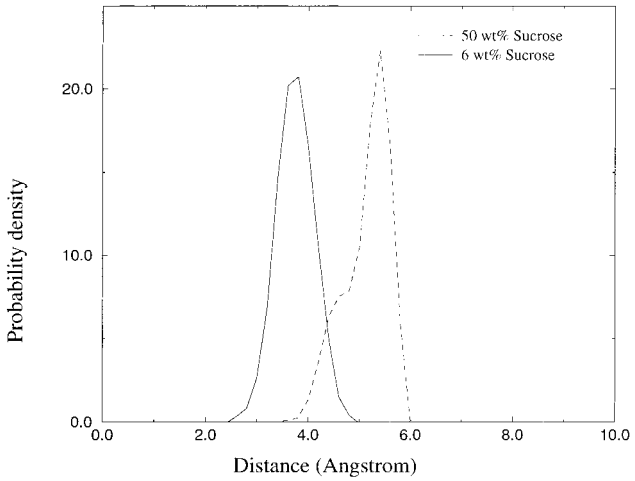

Figure 11. Probability distribution function for the intramolecular distance between O2 and O3′.

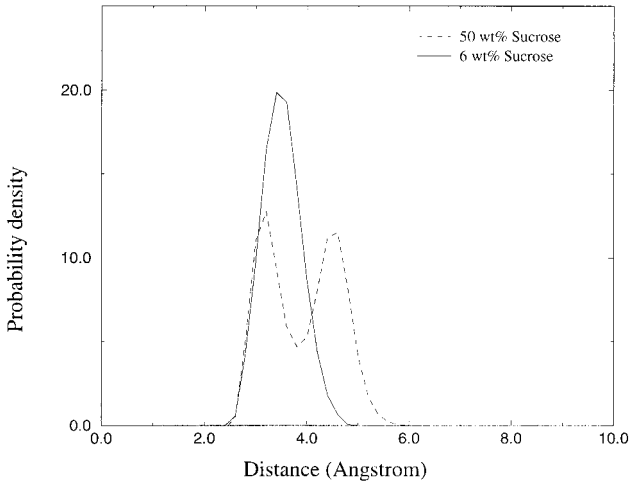

Figure 12. Probability distribution function for the intramolecular distance between O5 and O6′.

tempering simulations. It is apparent that the oscillations are more frequent for the parallel tempering run, which provides better sampling of configuration space.

The presence of intramolecular hydrogen bonds (H-bonds) can be detected by calculating a probability distribution between the two relevant oxygens. A peak between 3 and 4 Å implies the presence of an intramolecular H-bond if the angle H−O···H is 120° or greater.[31] Figure 11 shows the probability distribution of the distance between O3′ and O2′ (see Figure 1) for two different sucrose concentrations. In the 6 wt% solution, a peak at 3.8 Å and an H−O···H angle greater than 120° suggest that a hydrogen bond exists between the hydrogen on O3′ and O2. For the 50 wt% solution, the peak shifts to roughly 5 Å indicating that such a bond is no longer present. Figure 12 shows the probability distribution for the distance between O5 and O6′. The data suggest that the H-bond that forms between these two atoms is present in both dilute and concentrated solutions. In the concentrated case, a second peak indicates the presence of a second configuration which does not include this H-bond. Figure 13 shows the probability distribution of the distance between O2 and O2′. The three sets of data in the figure represent the 6 wt%, 50 wt% and 80 wt% solutions. In this case, no hydrogen bond is detected in the most dilute case (6 wt%). However, a bond begins to form at 50 wt%, as indicated by the small peak at about 3.0 Å. The presence of the hydrogen bond is more pronounced at the higher concentration (80 wt%).

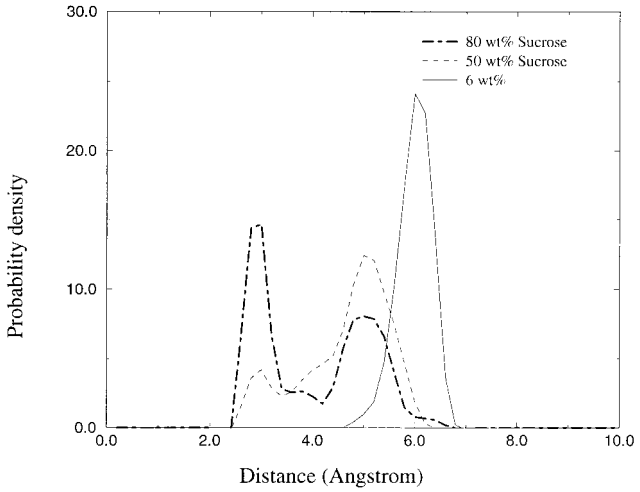

Figure 13. Probability distribution function for the intramolecular distance between O2 and O2′.

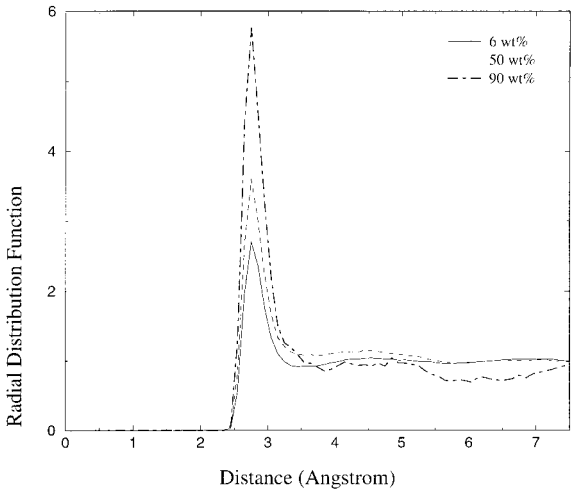

Figure 14. Radial distribution function between the oxygen on water molecules for different concentrations at 353 K.

Using X-ray crystallography, crystalline sucrose has been shown to have two intramolecular hydrogen bonds[28] (O6′−H···O5 and O2−H···O2′). Our data shows the presence of these two H-bonds at concentrations of 50 wt% sucrose and above (Figures 12, 13).

The addition of water to the sucrose system is known to disrupt the intraresidue hydrogen bonding.[13,32,33,34] Adams and co-workers saw no NMR evidence for the persistence of intramolecular hydrogen bonds in a dilute, 50 mM (∼ 1.7 wt%), sucrose in a water/acetone solution. Contrary to Adams' findings, Bock et al. showed that one hydrogen bond persisted (O6′−H···O5) while the O2−H···O2′ was replaced by O3′−H···O2. NOE and ^{13}C relaxation data supporting the rigidity of sucrose in dilute solutions have been obtained by McCain et al. The rigidity they observe has been attributed to the presence of intramolecular hydrogen bonds. In the 6 wt% sucrose simulations, the H-bond at O3′−H···O2 began to appear (see Figure 11) and the O6′−H···O5 H-bond persisted (Figure 12). Though, the O2−H···O2′ hydrogen bond was not detected (see Figure 13). Therefore, our results are consistent with both Bock et al. and McCain et al., who found that intramolecular H-bonds persist in 0.1 M (∼ 3.4 wt%) sucrose solutions. It is still conceivable, however, that at concentrations below 6 wt% all intramolecular H-bonds could disappear.

Therefore, unlike trehalose, which intramolecularly hydrogen bonds only at higher sugar concentrations (50 wt%),[17,35] sucrose remains hydrogen bonded in dilute solutions. How these intramolecular hydrogen bonds affect the sugar−water interaction is further discussed in the next section, where we examine the hydration of the disaccharides in different solutions.

3.2.2 Intermolecular Structure. The hydration number is defined as the average number of water molecules that are hydrogen bonded to a sucrose molecule. Similar to the discussion above, the criteria used are an oxygen−oxygen distance less than 3.4 Å and an H−O···O angle greater than 120°.[31] Figure 15 shows the hydration number as a function of sugar concentration for both sucrose and trehalose at 353 and 360 K, respectively. The sucrose hydration number gradually decreases with increasing concentration until a critical concentration near 50 wt%, where a sharp decrease in hydration number occurs. This faster decrease is probably due to the elimination of the hydration shell around the sucrose. It is interesting to note that this is the same concentration at which the molecules begin to resemble the H-bonded crystalline structures (as discussed above). The relative distribution of water in the bulk as opposed

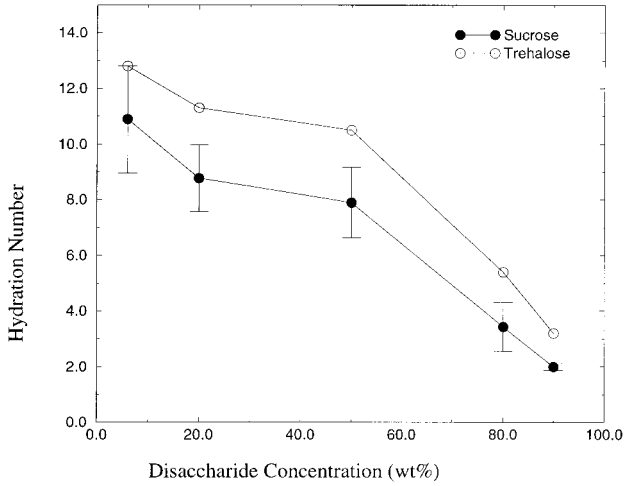

Figure 15. Hydration number as a function of increasing sugar concentration at 353 K for sucrose and 360 K for trehalose. Data points for the 80 and 90 wt% sucrose solutions are obtained using the parallel tempering method. The remaining points were calculated using conventional NPTMC. The trehalose data is from reference 17.

to the hydration shell changes with increasing concentration. For the dilute case (6 wt%), 11 out of 300 water molecules are involved in hydration as opposed to 16 out of 17 for the concentrated case (90 wt%). This "clustering" of water molecules becomes evident in the radial distribution data below.

Figure 14 shows the oxygen−oxygen radial distribution function for water. The peak at about 2.8 Å increases with increasing sucrose concentration. This result is consistent with the hydration number data, which show that the relative amount of water involved in the hydration shell increases with increasing sucrose concentration.

The hydration number calculated for the most dilute case (6 wt%) is 11.7. Previous sucrose hydration calculations used the hydration shell or separation distances of 2.8 to 3.7 Å as the criterion for hydration.[36] These criteria are not as strict as ours, so it is not surprising that the hydration numbers calculated here are smaller than those of others. Engelsen and co-workers calculated a hydration number of 24.7 by defining a hydration shell as all water molecules within 3.5 Å from a sucrose oxygen (3.7 wt% sucrose). When they altered their definition to all molecules within 2.8 Å, their hydration number dropped to 7. Using the Stokes−Einstein relationship and assuming a spherical solute geometry, a sucrose hydration of 5.3 has been reported.[28]

TABLE 2: Diffusion Coefficient Calculations for 80 wt% Sucrose Solutions

T (K)	time (ns)	D_{H_2O} (cm_2/s)	D_{suc} (cm^2/s)
400	22	$5.01(10^{-6})$	$8.614(10^{-8})$
450	22	$1.52(10^{-5})$	$4.59(10^{-7})$
500	6	$3.98(10^{-5})$	$1.524(10^{-6})$
600	5	$7.73(10^{-5})$	$5.223(10^{-6})$

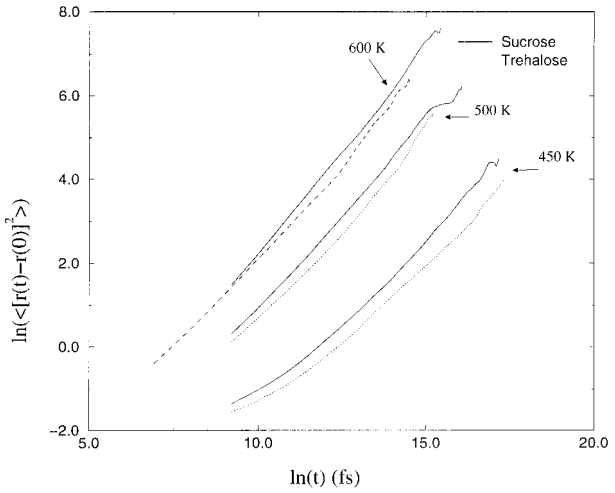

Figure 16. log−log plot of the mean squared displacement of sucrose and trehalose molecules as a function of time at different temperatures in an 80 wt% solution. Trehalose data were obtained from work done by Conrad and de Pablo.[17]

The hydration number for sucrose at infinite dilution was calculated at 13.9 using ultrasound measurements.[37] The inconsistencies in the hydration number calculation are largely due to the different definitions. It should also be noted that the above-mentioned studies were conducted on dilute sucrose systems (on the order 3−4 wt%). We find the method used in this work and also by Liu et al.[31] to be the most selective, as it only accounts for water molecules that are tightly hydrogen bonded to sucrose.

When compared with trehalose, sucrose is consistently less hydrated. This observation is related to the number of intramolecular hydrogen bonds found in trehalose and sucrose. Because trehalose forms only one intramolecular hydrogen bond,[17] as opposed to the two formed in sucrose, there are more sites available to hydrogen bond with water, resulting in a higher hydration number. Trehalose's unusual protectant capabilities could be partly due to its ability to bind water.

3.3 Diffusion Coefficient. Diffusion coefficients were determined from the mean squared displacement according to

$$6Dt = \langle |r_i(t) - r_i(0)|^2 \rangle \tag{13}$$

Diffusion coefficients were calculated for both the sucrose and the water in solution. The concentration of the sucrose−water systems was 80 wt%, and the temperatures were 300, 400, 450, 500, and 600 K. Lower temperatures were also attempted but, due to the slow dynamics, the diffusive regime could not be attained within a reasonable amount of computer time. Table 2 shows the sucrose and water diffusion coefficients at the different temperatures, along with the corresponding length of the run required to establish diffusion for sucrose. Figure 16 shows the mean squared displacement of sucrose and trehalose as a function of time. The slope at large times is unity, indicating that diffusion has been attained. At any given time, the sucrose trajectory is consistently higher than that of trehalose,

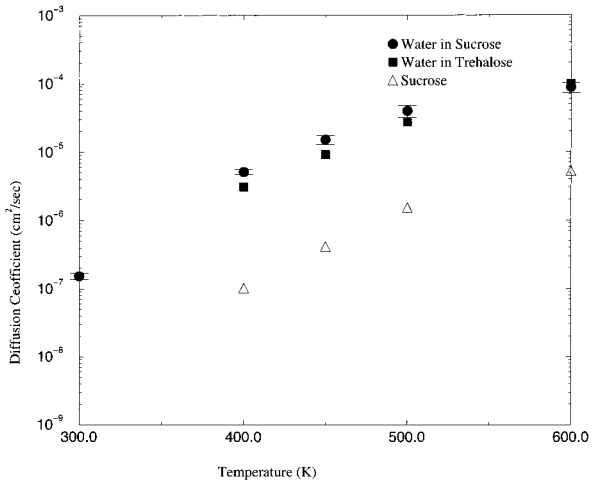

Figure 17. Diffusion coefficients of water in 80 wt% solutions of sucrose and trehalose and of sucrose in the same solution.

leading to greater diffusion coefficients. At the lowest temperature, the sucrose diffusion coefficient is approximately twice that of trehalose. The lower trehalose diffusion coefficient may be attributed to its larger hydration shell and higher density, as previously discussed. The bulkier water−trehalose complex would diffuse more slowly than the less hydrated sucrose. The higher densities observed for the trehalose solutions also lead to a decrease in sugar mobility which results in lower diffusion coefficients. The diffusion coefficients for water in both systems exhibit a similar trend, as shown in Figure 17; at lower temperatures, the diffusion coefficients in the sucrose solution are about 1.5 times higher than in trehalose, but are nearly equal at the higher temperatures. Since more water molecules are bound to trehalose than sucrose, their ability to diffuse is hindered, resulting in the lower diffusion coefficients in the trehalose solutions. Figure 17 also compares the sucrose and water diffusion coefficients. The diffusion coefficients for sucrose, as previously mentioned, are consistently lower than those of water. Interestingly, the magnitude of the difference in water and sucrose diffusion coefficients appears to increase as the temperature decreases.

The diffusion of pure sucrose was also calculated in a pure system. The simulated temperatures were 600, 520, and 450 K. Once again, sucrose has higher diffusion coefficients than trehalose (see Figure 18). This result can once again be attributed to the higher density of the trehalose system.

A simple Williams−Landel−Ferry[38] (WLF) equation can be applied to the sucrose data as shown in Figure 18. The WLF equation relates the temperature and the viscosity of near glassy systems as follows

$$\log \frac{\eta}{\eta_g} = \frac{-C_1(T - T_g)}{C_2 + (T - T_g)} \tag{14}$$

where η and η_g are the viscosities at temperatures T and T_g; and C_1 and C_2 are universal constants with values 17.44 and 51.6, respectively. To apply this equation to our systems, the viscosity was estimated from the Stokes−Einstein equation.

$$\eta = \frac{k_b T}{6\pi r D} \tag{15}$$

where k_b is the Boltzmann constant, r is the hydrodynamic radius, and D is the diffusion coefficient. The value for r is 3.35 and 3.78 for pure and 80 wt% sucrose, respectively; the

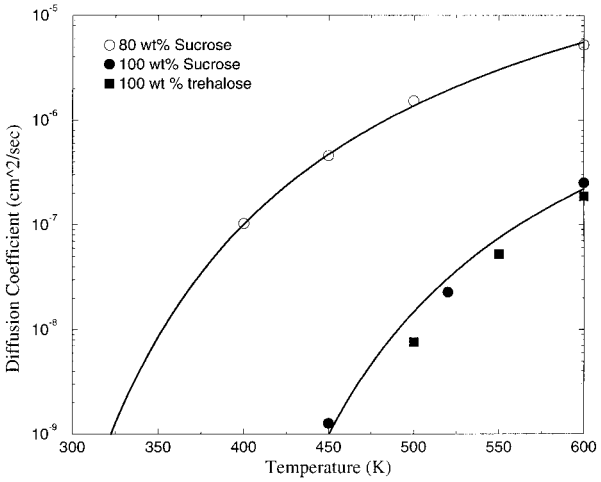

Figure 18. Diffusion coefficient for 80 wt% sucrose and pure sucrose at 353 K, and pure trehalose at 360 K.[17] The sucrose data has been fit to the WLF equation.

TABLE 3: VFT Parameters for 80 wt% and Pure Sucrose Solutions

system	B (K)	D_∞ (cm^2/sec)	T_o (K)
80 wt% (Fit)	1524	2.8×10^{-4}	209
80 wt% (WLF)	1519		193
100 wt% (Fit)	1162	3.0×10^{-6}	261
100 wt% (WLF)	1384		313

hydration shell is included in the 80 wt% radius calculation. The viscosity at the glass transition temperature (T_g) is determined using the relation developed by Soesanto and Williams[39] for concentrated fructose and glucose solutions.

$$\eta_g = 1.918x + 11.021 \tag{16}$$

where x is the mole fraction of sucrose. Using these three equations, we performed a nonlinear regression on the diffusion data for the 80 wt% and pure sucrose solutions. The T_g value was set at the experimental values of 235 and 350 K, respectively. The constants C_1 and C_2 were used as the fitting parameters. The C_1 and C_2 values calculated for the 80 wt% and pure systems were 15.674 and 42.100, and 16.313 and 36.847, respectively.

Alternatively, diffusion data can be interpreted in the context of the Vogel−Fulcher−Tamman (VFT) equation, given by

$$D(T) = D_\infty \exp\left[\frac{B}{T - T_o}\right] \tag{17}$$

where D_∞ is the diffusion coefficient at $T \rightarrow \infty$, B is the fragility parameter and T_o is the Vogel−Fulcher−Tamman temperature. The parameters that result from fitting the VFT equation to the 80 wt% and pure sucrose data are shown in Table 3.

Using the relations proposed by Fytas and co-workers,[40] the WLF parameters can be related to the VFT parameters by

$$B = 2.303C_1C_2 \tag{18}$$

$$T_o = T_g - C_2 \tag{19}$$

Table 3 shows the VFT parameter attained from fitting eq 17 to the diffusion data and the VFT parameter calculated using the WLF parameters according to eqs 18 and 19. The results as shown in Table 3 indicate that the WLF and VFT parameters are consistent. The relatively small values attained for B in the VFT equation and C_2 in the WLF equation both indicate that sucrose solutions form fragile glasses.[41] This is consistent with results reported by Miller and co-workers.[11] Through the application of the WLF or the VFT equation and the appropriate calculated parameters, it is possible to estimate the viscosities and diffusion coefficients of concentrated sugar solutions near the glass transition temperature. Such calculations are particularly important when designing freezing processes for biologicals in sugar solutions.

4. Conclusions

Simulation of sugar solutions near the glass transition temperature are often difficult due to the slow dynamics of the systems. Using a parallel tempering algorithm, which improves sampling of the configuration space, we were able to alleviate some of the problems associated with simulations of glassy systems. Density, hydration numbers, and structural information on 80, 90, and 100 wt% sucrose solutions were found consistent with experimental data. When sucrose and its solutions were compared with trehalose, the former demonstrated higher water diffusion coefficients, lower T_g, lower densities, and more intramolecular hydrogen bonding. Also, trehalose appears to exhibit a higher hydration number than sucrose. These characteristics play an important role in preservation processes. By binding water molecules more tightly, the glass formed by trehalose could hinder molecular motion more effectively, possibly leading to its superior cryo- and lyoprotection. We are currently applying parallel tempering to trehalose systems and trying to examine the differences between various disaccharides. This analysis will help explain the origin of trehalose's alleged superior performance as a preservation agent.

Acknowledgement. This work was supported by the Division of Chemical Sciences, Office of Basic Energy Sciences, and Office of Sciences at the U.S. Department of Energy. Acknowledgement is also made to the Donors of the Petroleum Research Fund, administered by the ACS, for partial support. N. Ekdawi-Sever received funding from The Biotechnology Training Program Fellowship sponsored by the National Institute of Health and from a Tau Beta Pi Fellowship.

References and Notes

(1) Schebor, C.; Burin, L.; Buera, M. P.; Aguilera, J. M.; Chirife, J. *Biotechnol. Prog.* **1997**, *13*(6), 857−863.
(2) Leslie, S. B.; Israeli, E.; Lighthart, B.; Crowe, J. H.; Crowe, L. M. *Appl. Environ. Microbiol.* **1995**, *61*(10), 3592−3597.
(3) Sun, W. Q.; Leopold, A. C.; Crowe, L. M.; Crowe, J. H. *Biophys. J.* **1996**, *70*, 1769−1776.
(4) Crowe, J. H.; Crowe, L. M.; Carpenter, J. J.; Rudolph, S. S.; Winstrom, C. A.; Spargo, B. J.; Anchordoguy, T. J. *Biochim. Biophys. Acta* **1988**, *947*, 367−384.
(5) Kob, W. *J. Phys.: Condens. Matter* **1999**, *11*, R85−R115.
(6) Mazzobre, M. F.; del Pilar Buera, M.; Chirife, J. *Lebensm. Wiss. Technol.* **1997**, *30*, 324−329.
(7) Rumsey, S. C.; Galeano, N. F.; Arad, Y.; Deckelbaum, R. J. *J. Lipid Res.* **1992**, *33*, 1551−1561.
(8) Moreira, T.; Pendas, J.; Gutierrez, A.; Pomes, R.; Duque, J.; Franks, F. *Cryo-Lett.* **1998**, *19*, 115−122.
(9) Lee, J. C.; Timasheff, S. N. *J. Biol. Chem.* **1981**, *256*(14), 7193−7201.
(10) Saleki-Gerhardt, A.; Zografi, G. *Pharm. Res.* **1994**, *11*(8), 1166−1173.
(11) Miller, D. P.; de Pablo, J. J.; Corti, H. *Pharm. Res.* **1997**.
(12) Rossi, S.; Buera, M. P.; Moreno, S.; Chirife, J. *Biotechnol. Prog.* **1997**, *13*, 609−616.
(13) Engelsen, S. B.; du Penhoat, C. H.; Perez, S. *J. Phys. Chem.* **1998**, *99*, 13334−13351.
(14) Bobrovnik, L. D.; Grekhov, A. M.; Gulyi, I. S. *J. Struct. Chem.* **1998**, *39*(5), 704−709.

(15) Roberts, C. J.; Debenedetti, P. G. *J. Phys. Chem. B* **1999**, *103*(34), 7308−7318.
(16) Caffarena, E. R.; Grigera, J. R. *Carbohydr. Res.* **1997**, *300*, 51−57.
(17) Conrad, P. B.; de Pablo, J. J. *J. Phys. Chem. A* **1999**.
(18) Hansmann, U. H. E. *Chem. Phys. Lett.* **1997**, *281*, 140−150.
(19) Berendsen, H. J. C.; Postma, J. P. M.; van Gunsteren, W. F.; Hermans, J.; D. Reidel Publishing Company, 1981; Chapter Interaction Models For Water In Relation To Protein Hydration, pages 331−342.
(20) Toukan, K.; Rahman, A. *Phys. Rev. B* **1985**, *31*(5), 2643−2648.
(21) Conrad, P. B.; de Pablo, J. J. *Fluid Phase Equilib.* **1998**, *150*−*151*, 51−61.
(22) Jorgensen, W. L.; Maxwell, D. S.; Tirado-Rives, J. *J. Am. Chem. Soc.* **1996**, *118*, 11225−11236.
(23) Essmann, U.; Perera, L.; Berkowitz, M. L. *J. Chem. Phys* **1995**, *103*(19), 8577−8593.
(24) Mehlig, B.; Heermann, D. W.; Forrest, B. M. *Phys. Rev. B* **1992**, *45*(2), 679−685.
(25) Nosé, S. *Prog. Theor. Phys. Supp.* **1991**, (103), 1−46.
(26) Martyna, G. J.; Tucherman, M. E.; Tobias, D. J.; Klein, M. L. *Mol. Phys.* **1996**, *87*(5), 1117−1157.
(27) Tuckerman, M.; Berne, B. J.; Martyna, G. *J. Chem. Phys.* **1992**, *97*(3), 1990−2001.
(28) Mathlouthi, M.; Reiser, P., Eds. *Sucrose Properties and Applications;* Blackie Academic & Professional, 1st ed., 1995.
(29) Shamblin, S. L.; Taylor, L. S.; Zografi, G. *J. Pharm. Sci.* **1998**, *87*(6), 694−701.
(30) Ding, S. P.; Fan, J.; Green, J. L.; Lu, Q.; Sanchez, E.; Angell, C. A. *J. Therm. Anal.* **1996**, *47*, 1391−1405.
(31) Liu, Q.; Schmidt, R. K.; Teo, B.; Karplus, P. A.; Brady, J. W. *J. Am. Chem. Soc.* **1997**, *119*, 7851−7862.
(32) Adams, B.; Lerner, L. *J. Am. Chem. Soc.* **1992**, *114*, 4827−4829.
(33) McCain, D. C.; Markley, J. L. *J. Am. Chem. Soc.* **1986**, *108*, 4259−4264.
(34) Bock, K.; Lemieux, R. U. *Carbohydr. Res.* **1982**, *100*, 63−74.
(35) Magazu, S.; Maisano, G.; Middendorf, H. D.; Migliardo, P.; Musolino, A. M.; Villari, V. *J. Phys. Chem.* **1998**, *102*, 2060−2063.
(36) Engelsen, S. B.; Perez, S. *Carbohydr. Res.* **1996**, *292*, 21−38.
(37) Galema, S. A.; Høiland, H. *J. Phys. Chem.* **1991**, *95*, 5321−5326.
(38) Williams, M. L.; Landel, R. F.; Ferry, J. D. *J. Am. Chem. Soc.* **1955**, *77*, 3701−3706.
(39) Soesanto, T.; Williams, M. C. *J. Phys. Chem.* **1981**, *85*, 3338−3341.
(40) Fytas, G.; Patkowski, A.; Meier, G.; Dorfmüller, T. *J. Chem. Phys.* **1984**, *80*(5), 2214−2220.
(41) Angell, C. A. *Polymer* **1997**, *38*(26), 6261−6266.